Journal of Mechanical Science and Technology 00 (0) 2019

Original Article
DOI 10.1007/s12206-000-0000-0

Keywords:
· Euler-Bernoulli beam
· Flow-structure interaction
· Resonance
· Vortex street

Correspondence to:
Anne Cros
anne.cros@academicos.udg.mx

Citation:

Sandoval Hernández, E., Llewellyn Smith, S. G., Cros, A. (2019) Resonance of a flexible plate immersed in a von Kármán street. Journal of Mechanical Science and Technology 00 (0) (2019) 0000~0000. http://doi.org/10.1007/s12206-000-0000-0

Received please leave blank

Revised please leave blank

Accepted please leave blank

† Recommended by Editor
please leave blank

Resonance of a flexible plate immersed in a von Kármán vortex street

Erika Sandoval Hernández[1], Stefan G. Llewellyn Smith[2,3] and Anne Cros[4*]

[1,4]Physics Department CUCEI, Universidad de Guadalajara, Guadalajara, Jal. 44430, Mexico, [2]Department of Mechanical and Aerospace Engineering, Jacobs School of Engineering, UCSD, La Jolla CA 92093-0411, USA, [3]Scripps Institution of Oceanography, UCSD, La Jolla CA 92093-0230, USA

Abstract This work presents a theoretical and experimental study of a flexible plate immersed in a von Kármán vortex street. The wake is generated in a water flow using a cylindrical obstacle with a Reynolds number lower than 200. The vortices provoke oscillations of a flexible plate whose leading edge is clamped a few cylinder diameters downstream of the obstacle. The oscillation amplitude of the free edge is examined experimentally as the plate length is varied with respect to the wavelength. The value of the peak of the amplitude and the phase shift between the forcing vortices and the plate deflection are consistent with theoretical predictions. These predictions use an Euler-Bernoulli model for the motion of the plate produced by the pressure difference over the plate due to the combined effect of the vortex street and the deflection of the plate. The ratio between the plate length and the wake wavelength for which resonance occurs is fixed by the condition that the natural frequency of the plate is equal to the vortex frequency.

1. Introduction

A flexible plate can spontaneously flutter when it is immersed in a steady, laminar flow with high enough velocity [1]. The corresponding aeroelastic instability arises from a competition between the stabilizing effect of the plate rigidity and destabilizing pressure fluctuations. However, a periodic flow with mean intensity much lower than the steady instability threshold can also induce periodic pressure fluctuations that are sufficient to induce oscillations of the plate. This is the case of an array of vortices shed periodically from an upstream obstacle, the von Kármán vortex street.

Recent studies have shown that the energy of the vortices in a von Kármán street can be harvested using piezoelectric converters embedded in a flexible plate which vibrates because of the wake. One of the first experimental works [2] showed that the amplitude of the free trailing edge is maximum when the oncoming vortex frequency has the same value as the natural frequency of the plate first mode, i.e. there is resonance. This result was confirmed by further studies [3, 4, 5].

The vortex street energy can also be extracted by some fish when they swim downstream of an obstacle [6]. The swimming dynamics of the fish then completely changes as the fish slaloms in the oncoming vortices and activates only its anterior axial muscles [7]. Even a passive body can be propelled upstream, developing thrust and overcoming its own drag, as observed for a dead fish [8] and for an articulated fish-like system [9].

The influence of the governing parameters was studied by different authors [10] showing that, depending on the Reynolds number, the plate could flap in different ways: like a cantilever, with a combination of traveling waves, or quasi-periodically. This latter regime is promoted by higher chord-to-span ratio values thanks to the appearance of three-dimensional effects [11]. [12] established that a flag whose leading edge has a finite diameter could generate vortices which would induce ``forced flapping'' as soon as $Re \gtrsim 100$. Whereas several authors found that vor-

tices are shed when the plate is fixed to a cylinder axis [13], the numerical study of [14] showed that the ``vortex street mode'' develops only when the flag is placed further from the cylinder.

Several theoretical studies have examined the mutual interaction between the vortex street and a flexible body immersed inside it. [2] described the traveling waves that develop in large flexible plates as a superposition of the first four modes observed in flutter. They calculated each mode's amplitude by solving an Euler-Bernoulli equation governing the oscillations of the plate. [12] studied the influence of a flagpole subject to aeroelastic instability. These authors used the Bernoulli equation with a tension term and studied the solutions of the linearized equation. They did not take into account the modification of the flow due to the plate oscillations, as done by [15], who estimated the pressure distribution on the edges of the plate from the velocity fields generated by a point vortex model taking into account the deflection of the plate. The present theoretical model is based on a corrected version of the work of [15] and [16] and adapted to our experimental conditions to describe the resonance that occurs in our system. The corrected version does not use an incorrect decomposition of the problem into two sub-problems.

Resonance is a phenomenon that occurs in different systems such as the parametric mechanical pendulum [17], electrical circuits [18], stationary waves in wind and string instruments [19] and on the surface of a liquid [20]. For all these cases, the system parameters set the natural frequency f_0. In the last two cases, the spatial size S of the system allows to find a discrete number of resonant wavelengths ℓ_i; for example $S = i\ell_i/2, i \in \mathbb{N}$ for Dirichlet boundary conditions in a one-dimensional system. The wavelengths are then related to the temporal resonant frequencies f_{0i} by the dispersion relation.

The von Kármán vortex street generates a temporally as well as spatially periodic pattern with respective frequencies f and λ. Although a number of studies of flexible plates oscillating inside a von Kármán street have reported a maximum amplitude when the excitation and natural frequencies coincide, no work to date has specifically examined the influence of the spatial structure of the vortex street along the chord of the plate. In this experimental and theoretical work, the plate and the vortex street oscillate at the same frequency in any case. Instead, the plate chord is varied while the von Kármán street is left unchanged. The amplitude of the plate's trailing edge is obtained for different plate chords, and the phase shift between the vortices and the plate trailing edge is estimated.

Section 2 describes the experimental setup and the methodology used to visualize both the vortices and the plate's deflection. The mathematical model of the interaction between the flexible structure and the von Kármán street is presented in Section 3. Section 4 discusses the results, while Section 5 ends the paper with conclusions.

2. Experiment

The experiments are performed in a water channel with test section dimensions $0.10 \times 0.10 \times 1.00\ m^3$. The overall device is shown in Fig. 1. The water flow is generated by a pump controlled by a variable-frequency drive. Before the test section, convergent and honeycomb panels enforce laminar flow. The von Kármán street is generated thanks to a cylindrical obstacle (diameter $D = 1.25$ cm). The plate's leading edge is clamped to a thin vertical axis (diameter 0.3 mm) five diameters downstream of the cylinder to avoid suction effects. The characteristics of the flexible plate are shown in Table 1. Its flexural rigidity $B = \frac{Ye^3}{12(1-\nu^2)}$ was determined from the plate's natural frequency in air, where Y is the Young modulus, e is the plate thickness and ν the Poisson coefficient. Fig. 2 shows the free extreme transverse displacement of 10.0 cm-long plate when it is released after an initial deflection. In the experiment, the plate's trailing edge is left free. The plate material has a density close to that of water and its elasticity is high enough to avoid nonlinear high-amplitude motions, while at the same time it is flexible enough to be displaced by the vortices. Tin and copper electrodes are placed upstream and downstream of the obstacle and the flexible plate, respectively, to generate white tin oxide which is advected by the flow [21]. Using this procedure the vortices appear as dark regions surrounded by clearer tin oxide lines as in Fig. 3.

A Nikon videocamera is placed above the system, allowing us to record the vortices and the flexible plate simultaneously. The frame size is 1080×1800 pixels with a resolution of 10 pixels per millimeter. Videos were recorded over a period of 300 s. A spatiotemporal diagram was then extracted, with abscissa representing time and ordinate corresponding to the

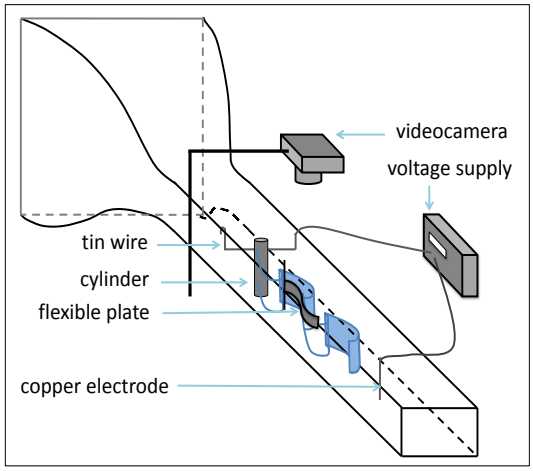

Fig. 1. Experimental setup.

Table 1. Flexible plate characteristics.

chord length 2L (cm)	span H (cm)	mass per area unit ρ_s (g/m²)	flexural rigidity B (N.m)
$(5.0 - 10.5) \pm 0.1$	2.0 ± 0.1	34	8.1×10^{-5}

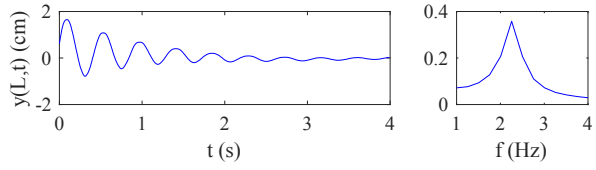

Fig. 2. Free oscillations in air of the plate's free end when the other end is clamped for $2L = 10.0$ cm (left). Right: Fourier spectrum.

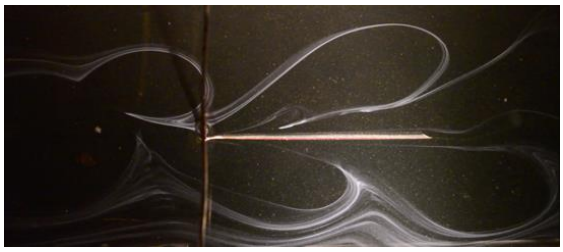

Fig. 3. Image of the flow near the flexible plate. The cylinder which generates the vortices is barely visible on the left-hand side of the picture. The vertical wire constrains the axis of the plate's leading edge.

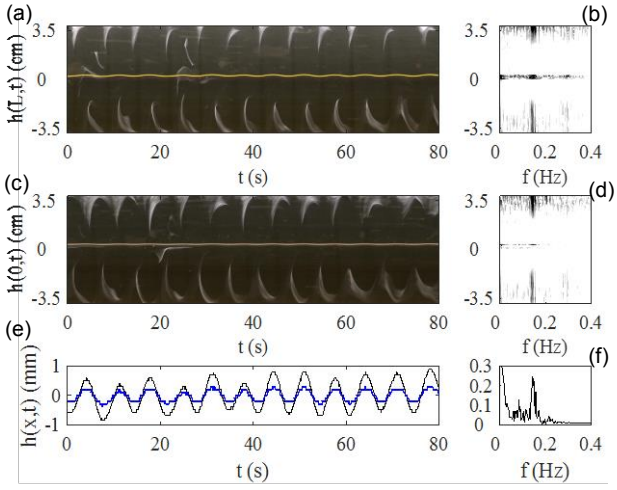

Fig. 4. Spatiotemporal diagrams for $2L = 8.0$ cm (corresponding to $2L/\lambda = 1.07$, where λ is the vortex street wavelength) performed at the trailing edge (a) and at the plate midpoint (c) with their respective Fourier spectra in (b) and (d). (e) Oscillations of the plate's free end (black curve) and of its middle (blue curve). (f) Fourier spectrum of the oscillations of the free edge (performed over 300 s). The low frequency peak near $f = 0$ corresponds to a slight displacement of the plate's free end mean position along the acquisition time.

pixel values along a vertical line passing through the free edge of the plate. An example is shown in Fig. 4(a). The corresponding Fourier spectrum performed along each line of the diagram is shown in Fig. 4(b).

The spectrum allows us to determine the vortex frequency and to compare it to the plate's frequency of oscillation. The oscillations of the plate's free edge can also be extracted from the spatiotemporal diagram, as shown in Fig. 4(e). The oscillation of the middle-chord of the plate can be observed in the same figure in blue: it shows that all the points along the plate oscillate with the same phase. This observation is in agreement with the results of [10]. From this plot, both the temporal frequency and the amplitude of the plate's oscillation can be determined.

The experimental protocol is as follows. The longest $(2L/\lambda = 1.4)$ flexible plate is clamped along its leading edge and immersed into the von Kármán street. After several minutes to allow transients to decay, the power supply is switched on to generate the tin oxide and a video is recorded over 5 minutes. Then the flexible plate is cut by 5 mm and the same process is repeated. It is important to note that the flow

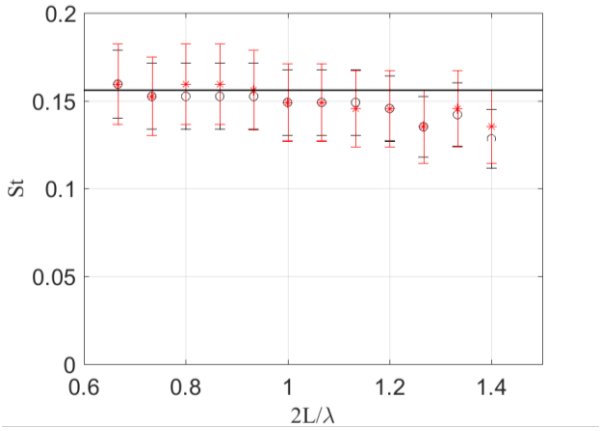

Fig. 5. Frequency of the plate's largest oscillations (black, empty circles) and of the vortices (red stars). Error bars denote a confidence level of 95%. Continuous line: Strouhal number predicted by [22].

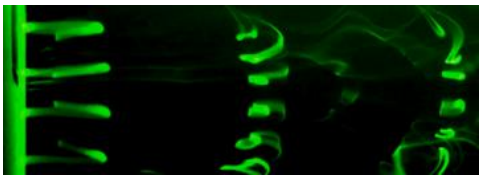

Fig. 6. Side view of the vortices which shed parallel to the cylinder axis. The image height is approximately equal to 7 cm.

velocity is left constant for all the experiments and equal to 1.2 cm/s, so that the Reynolds number calculated from the obstacle diameter D is equal to $Re = 148$.

As mentioned before, the tin oxide method allows us to visualize the Kármán vortices and to compare the experimental characteristics of the wake with the literature. The experimental wavelength was found to be $\lambda = 6D$, which is slightly greater than the values given by [23] and [24] of $4D$ and $5D$ respectively. The frequencies of motion of the plate and of the vortices are deduced from the Fourier spectra of Fig. 4(b) and (d); their dependence on the plate chord is shown in Fig. 5, where $St = \frac{fD}{v}$ is the classical Strouhal number calculated from the obstacle diameter. Both values are equal to the result of [22] for $\mathrm{Re} = 148$ whereas a slight decrease is observed when the plate length is increased. Fig. 6 shows that the vortices can be considered parallel to the cylinder axis.

3. Mathematical model

We model a flexible plate immersed in a vortex street, as illustrated in Fig. 7. A plate of chord $2L$ is immersed in a flow with background velocity U. A vortex street is present in the flow, characterized by its wavelength λ, frequency $\omega = 2\pi f$ and the distance d between the two vortex rows. Unlike in [2], the agreement between plate and vortex frequencies seen in Fig. 5 leads us to adapt the model of [15], in which only a single frequency is considered, to our experimental conditions.

In this model the origin $(x = 0)$ is at the middle of the plate. The vortices have circulation $\pm\Gamma$ (where $\Gamma < 0$ for the classical vortex street) and induce on the centreline $y = 0$ the velocity components

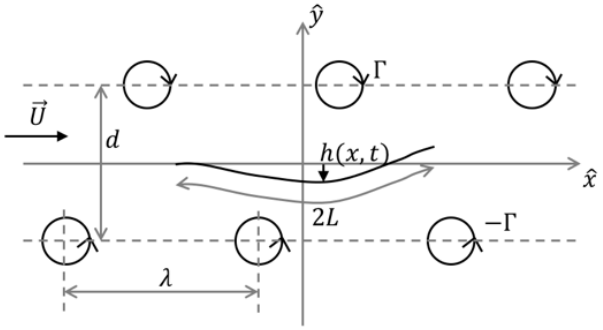

Fig. 7. Illustration of the model.

$$u_m = U + \frac{\Gamma}{\lambda};\ v_m(x,t) = \frac{2\Gamma}{\lambda} e^{-\frac{\pi d}{\lambda}} \sin\left[2\pi\left(\frac{x - U_c t}{\lambda}\right)\right]. \tag{1}$$

Note that the horizontal velocity is steady and uniform in x. The translation velocity of the vortices U_c is related to the fluid velocity U by

$$U_c = U + \frac{\Gamma}{2\lambda}\tanh\left(\frac{\pi d}{\lambda}\right) \sim U + \frac{\Gamma}{2\lambda} \tag{2}$$

where the final expression corresponds to the limit $\pi d/\lambda \gg 1$, which is appropriate here. The angular frequency of the vortices' motion past a fixed point $\omega = 2\pi f$ is related to their translation velocity U_c and wavelength λ by

$$\omega = \frac{2\pi U_c}{\lambda}. \tag{3}$$

We define a non-dimensional frequency Ω by

$$\Omega = \frac{\omega L}{u_m} = \frac{2\pi U_c}{u_m}\frac{L}{\lambda} \tag{4}$$

where u_m is the fluid velocity on the plate given in Eq. (1).

We now follow [16,15] and obtain a mathematical model for the oscillation of the plate in the flow. Taking the plate displacement to be formally small, we linearize the problem. Then the solution is periodic with frequency ω, so that we adopt complex notation with the real part understood. The total circulation in the wake is periodic and advected downstream, so that

$$\Gamma(x,t) = \Gamma_0 e^{i\omega t} e^{-\frac{i\omega(x-L)}{u_m}} \tag{5}$$

for $L < x$. We now use non-dimensional variables, scaling lengths by L and time by λ/U_c. The transversal component of velocity on the plate becomes $v_m(x,t) = V_m(x)e^{i\omega t}$, and from Eq. (1),

$$V_m(x) = 2i\frac{\Gamma/\lambda U}{1 + \frac{1}{2}(\Gamma/\lambda U)}\frac{\lambda}{L} e^{-\frac{2i\pi x L}{\lambda}} e^{-\frac{\pi d}{\lambda}} = iV_0 e^{-\frac{2i\pi x L}{\lambda}}. \tag{6}$$

The condition of no normal flow through the plate leads to a relationship between the circulation and transversal velocity:

$$\frac{1}{2\pi}\int_{-1}^{1}\frac{G(x')}{(x-x')}\,dx' = 2i\pi\, H(x) + \frac{u_m}{U_c}\frac{\lambda}{L}H'(x) - V_m(x) - \Gamma_0 E(x) \quad \text{for } -1 < x < 1, \tag{7}$$

where $G(x)$ is the vortex sheet strength and

$$E(x) = -\frac{i\Omega}{2\pi}\frac{\int_1^\infty e^{-i\Omega(x'-1)}}{x - x'}dx' \tag{8}$$

is a known function representing the known circulation in the wake and $H(x)$ is the deflection of the plate. The function $G(x)$ and Γ_0 are unknown at this point. The equation (3.7) in [15] that corresponds to Eq. (7) above has U rather than u_m in front of the H' term, which is incorrect as the horizontal velocity on the plate is u_m and not U.

Evaluating the pressure on both sides of the body leads to a relation between G and the pressure jump P:

$$\partial_x P = 2i\pi G + \frac{1 + \Gamma/\lambda U}{1 + \frac{1}{2}(\Gamma/\lambda U)}\frac{\lambda}{L}\partial_x G. \tag{9}$$

This equation can be integrated to give

$$P(x) = 2i\pi\int_1^x G(x')\,dx' + \frac{1 + \frac{\Gamma}{\lambda U}}{1 + \frac{1}{2}\left(\frac{\Gamma}{\lambda U}\right)}\frac{\lambda}{L}(G(x) + i\Omega\Gamma_0), \tag{10}$$

taking P to vanish at the trailing edge and using $G(1) = -i\Omega\Gamma_0$. We define the two nondimensional numbers R_1 and R_2 as

$$R_1 = \frac{\rho_s}{\rho_f L};\qquad R_2 = \frac{B}{\rho_f {U_c}^2 L^3}\frac{\lambda^2}{L^2}, \tag{11}$$

ρ_f is the fluid density in kg/m^3, ρ_s the plate mass density per unit of area in kg/m^2 and B is the plate flexural rigidity. The plate deflection then satisfies

$$-(2\pi)^2 R_1 H + R_2 H_{xxxx} = -P, \tag{12}$$

with boundary conditions

$$H(-1) = H_0 e^{i\phi_H},\qquad H'(-1) = \Theta e^{i\phi_\theta},\qquad H''(1) = H'''(1) = 0, \tag{13}$$

where H_0 and Θ are the imposed amplitudes of the heaving and pitching motions at the leading edge respectively. Here $H_0 = \Theta = 0$ since the plate is clamped. The deflection $H = \|H\|e^{i\phi}$ is a complex quantity with a phase ϕ that vanishes when an upper vortex passes above the midpoint of the plate.

This is essentially the same problem as [15], who outlines a solution procedure that decomposes it into two sub-problems, one without body motion and the other with the vortex street as investigated in [16]. However, Eq. (3.9) in [15] governing the latter problem is incorrect, and the two sub-problems cannot be decoupled in the suggested fashion.

We solve the full system given above using a version of the numerical approach of §2 of [15], which is explained in more detail in §5 of [16]. The full procedure is given there and is applicable to the current problem; it is just the decomposition mentioned above that is incorrect. Briefly, the approach is to solve for $V(x)$ and $H''(x)$ on the plate, along with Γ_0. The functions $V(x)$ and $H''(x)$ are discretized using $m+1$ Chebyshev-Lobatto nodes over the interval $(-1,1)$, yielding a total of $2m+3$ unknowns. These are updated using an iterative approach. Given $H''(x)$, the deflection $H(x)$ is obtained by integration with the two boundary conditions at $x=-1$. One can then compute $V(x)$ from Eq. (7). The $2m+3$ equations to be solved correspond to zeroing out the difference between the two discretized versions of $V(x)$ on the $m+1$ points, the plate Eq. (12) over the $m-1$ interior points, and the two free edge conditions for the plate at $x=1$. This is done using Brouder's algorithm. [15] was followed to deal with the logarithmic singularity of $F(x)$ near $x=1$, but this was not essential.

The parameters used in the numerical algorithm are R_1, R_2, Ω, λ/L and V_0. These are not independent parameters in this problem. Dimensional considerations show that there are seven dimensional input quantities, B, ρ_s, ρ_f, L, D, U and ν (we ignore three-dimensional effects and hence H). Of the four resulting nondimensional parameters, three are set by the experimental design: R_1, L/D and $\mathrm{Re}=UD/\nu$. The fourth parameter, R_2, is defined in terms of further parameters as follows. The fluid problem depends only on Re, implying that $\lambda/D = g_\lambda(\mathrm{Re})$, $\frac{d}{D} = g_d(\mathrm{Re})$ and $\Gamma/UD = g_\Gamma(\mathrm{Re})$. The distance d/D and wavelength λ/D are taken as the experimentally-measured values $d=3.6D$ and $\lambda=6D$, while the circulation $\Gamma=-\pi UD$ following [25]. We can now obtain U_c, R_2 and u_m from Eqs. (2), (11) and (1) respectively. Finally we obtain Ω and V_0 from Eqs. (4) and (6).

4. Results

The amplitude of the motion of the free edge is shown in Fig. 8(a), together with the predictions of the theoretical model. The upper x-axis gives the ratio of the frequency of the fundamental mode of the plate in water, f_P, to the vortex frequency, f_V. Note that the f_P values vary from 0.11 Hz for the longest plate to 0.50 Hz for the shortest one. These values are lower than the natural frequencies in air (see Fig. 2) because of the added mass of water. It can be seen that, as in previous works, the amplitude is maximal for $f_P/f_v \cong 1$.

The phase shift ϕ between the plate and the vortices crossing its midpoint is shown in Fig. 8(b). The phase was estimated from the correlation between the plate deflection, $h(L,t)$, and a line of pixels extracted from the spatio-temporal diagrams performed at $x=0$ and $y\cong 3$ cm. Fig. 9 shows two examples of correlation functions. The downward-pointing peaks correspond to the clearest pixels indicating the absence of vortices. The midpoint and trailing edge lines of pixels are not exactly the same, despite the similarities of Fig. 4(a) and (c). This suggests that the motion of the vortices is being perturbed by the flow induced by the plate, an effect not included in the theoretical model. The theoretical phase in Fig. 8(b) is shifted by π in order to take into account the offset between the top and bottom row of vortices. Since the forcing vortices are distributed in space, the phase difference does not have a jump near the amplitude resonance. There is a gradual decrease in phase, seen in both theoretical and experimental results.

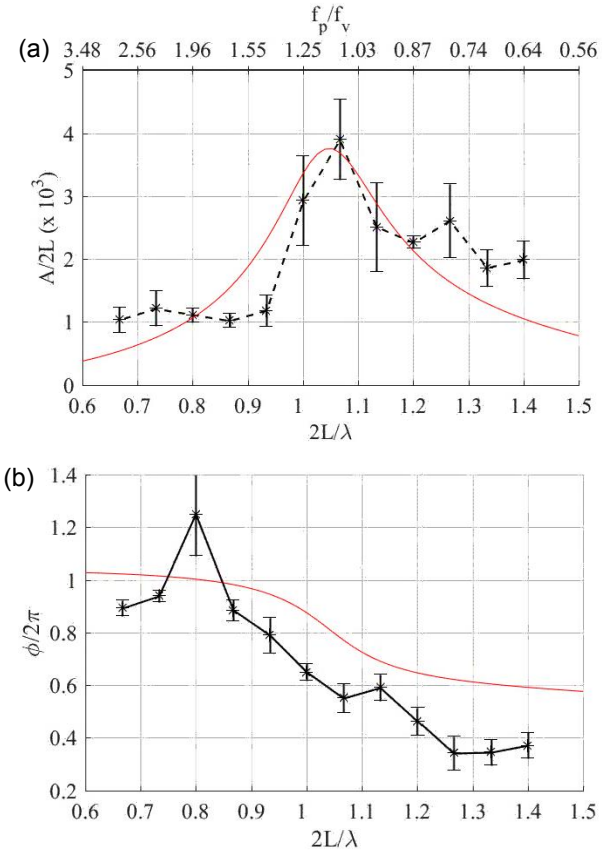

Fig. 8. Amplitude of the oscillations of the plate's free edge (a) and phase difference between the plate and the vortices at the midpoint (b) as a function of its nondimensional length. Red solid curve: theoretical predictions; black curve with error bars and stars: experimental measurements. Error bars denote a confidence level of 95%.

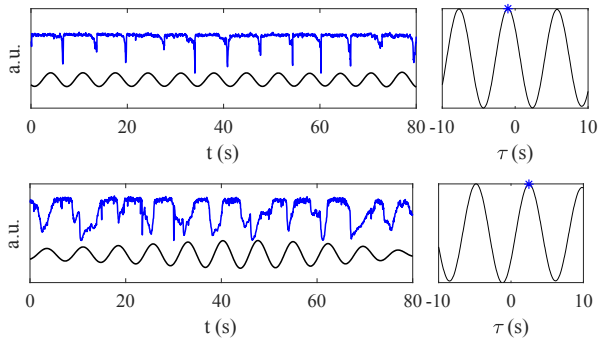

Fig. 9.Left plots: temporal evolution of the plate midpoint oscillation $h(L,t)$ (black) and the intensity level of a line of the spatio-temporal diagram at $y=3$ cm, $x=0$ (blue). Right: correlation functions between the two functions with the maximum (*). Top: $2L/\lambda=0.87$; bottom: $2L/\lambda=1.27$.

3. Conclusions

The phenomenon of resonance between a flexible plate immersed in a von Kármán street and the oncoming vortices was investigated. Both the vortices and the plate deflection are visualized in a water channel for $\mathrm{Re} = 148$. The leading edge of the plate is clamped downstream of the cylindrical obstacle which generates the vortex street. The forcing is both spatially and temporally periodic, and the influence of the ratio $2L/\lambda$ between the plate chord and the wake wavelength is studied. A resonance occurs at a specific value of $2L/\lambda$ corresponding to when the natural frequency of the plate in water corresponds to the vortex street frequency. The resonance was identified by maximum in the deflection amplitude of the plate's free end. The phase response is more complicated and shows a gradual change across the resonance, presumably due to the internal degrees of freedom of the system. Both amplitude and phase results are in agreement with the theoretical model of an Euler-Bernoulli beam immersed inside a fluid containing an array of point vortex. The model developed by [15] was corrected by not using two decoupled sub-problems. The plate motions are due to the pressure fluctuations over its two faces, which are generated by the vortex array and the deflection of the plate. As resonance appears to play an important role in the transition from drag to thrust [15], the force should change of sign for the range of parameters explored here, but this experimental measurement requires sensitive measurements and is beyond the scope of the present work.

Acknowledgment

This work was supported by CONACyT (CB-2008-1 #103941 and A1-S-55355), Mexico, and by UC-Mexus and CONACyT ("Sky dancer: a complex system of fluid-structure interaction").

Nomenclature

$2L$	: plate length
B	: plate flexural rigidity
ρ_s	: plate mass density
U	: fluid velocity
ρ_f	: fluid density
λ	: vortex wavelength
d	: vortex row separation
Γ	: vortex circulation
U_C	: vortex translation velocity
u_m	: longitudinal component of the fluid velocity on the plate
v_m	: transversal component of the fluid velocity on the plate

References

[1] C. Eloy, C. Souilliez, and L. Schouveiler, Flutter of a rectangular plate, *Journal of Fluids and Structures*, 23(6) (2007) 904-919.

[2] J. J. Allen, and A. J. Smits, Energy harvesting eel. *Journal of Fluids and Structures*,15(3-4) (2001) 629-640.

[3] H. D. Akaydın, N. Elvin, and Y. Andreopoulos, Wake of a cylinder: a paradigm for energy harvesting with piezoelectric materials, *Experiments in Fluids*, 49(1) (2010) 291-304

[4] X. Gao, W. H. Shih, and W. Y Shih,. Flow energy harvesting using piezoelectric cantilevers with cylindrical extension, *IEEE Transactions on Industrial Electronics*, 60(3) (2012) 1116-1118.

[5] M. Demori, M. Ferrari, A. Bonzanini, P. Poesio, and V. Ferrari, Autonomous Sensors Powered by Energy Harvesting from von Karman Vortices in Airflow, *Sensors*, 17(9) (2017) 2100.

[6] J. C. Liao, D. N. Beal, G. V. Lauder, and M. S. Triantafyllou, The Kármán gait: novel body kinematics of rainbow trout swimming in a vortex street, *Journal of experimental biology*, 206(6) (2003) 1059-1073.

[7] J. C. Liao, D. N. Beal, G. V. Lauder, and M. S. Triantafyllou, Fish exploiting vortices decrease muscle activity, *Science*, 302 (5650) (2003) 1566-1569.

[8] D. N. Beal, F. S. Hover, M. S. Triantafyllou, J. C. Liao, and G. V. Lauder, Passive propulsion in vortex wakes, *Journal of Fluid Mechanics*, 549 (2006) 385-402.

[9] J. D. Eldredge, and D. Pisani, Passive locomotion of a simple articulated fish-like system in the wake of an obstacle, *Journal of Fluid Mechanics*, 607 (2008) 279-288.

[10] S. Shi, T. H. New, and Y. Liu, Flapping dynamics of a low aspect-ratio energy-harvesting membrane immersed in a square cylinder wake, *Experimental Thermal and Fluid Science*, 46 (2013) 151-161.

[11] S. Shi, T. H. New, and Y. Liu, Effects of aspect-ratio on the flapping behaviour of energy-harvesting membrane, *Experimental Thermal and Fluid Science*, 52 (2014) 339-346.

[12] A. Manela, and M. S. Howe, The forced motion of a flag, *Journal of Fluid Mechanics*, 635 (2009) 439-454.

[13] A. K. Soti, R. Bhardwaj, and J. Sheridan, Flow-induced deformation of a flexible thin structure as manifestation of heat transfer enhancement, *International Journal of Heat and Mass Transfer*, 84 (2015) 1070-1081.

[14] D. Pan, X. Shao, J. Deng, and Z. Yu, Simulations of passive oscillation of a flexible plate in the wake of a cylinder by immersed boundary method, *European Journal of Mechanics-B/Fluids*, 46 (2014) 17-27.

[15] S. Alben, Passive and active bodies in vortex-street wakes, *Journal of Fluid Mechanics*, 642 (2010) 95-125.

[16] S. Alben, Optimal flexibility of a flapping appendage in an inviscid fluid, *Journal of Fluid Mechanics*, 614 (2008) 355-380.

[17] G. L. Baker, and J. A. Blackburn, *The pendulum: a case study in physics*. Oxford University Press, New York, USA, (2005).

[18] D. Chattopadhyay, *Electronics (fundamentals and applications),* 7th Ed. New Age International, New Delhi, India, (2006).

[19] N. H., Fletcher, and T. D. Rossing, *The Physics of Musical Instruments,* 2nd Ed. Springer, New York, USA, (1998).

[20]L. M. Milne-Thomson, *Theoretical Hydrodynamics*, 5th Ed. Dover Publications Inc., New York, USA, (1962).
[21]S. Taneda, Visual study of unsteady separated flows around bodies, *Progress in Aerospace Sciences*, 17 (1977) 287-348.
[22]C. H. Williamson, Oblique and parallel modes of vortex shedding in the wake of a circular cylinder at low Reynolds numbers, *Journal of Fluid Mechanics*, 206 (1989) 579-627.
[23]T. Karasudani, and M. Funakoshi, Evolution of a vortex street in the far wake of a cylinder, *Fluid Dynamics Research,* 14(6) (1994) 331.
[24]P. G. Saffman, and J. C. Schatzman, An inviscid model for the vortex-street wake, *Journal of Fluid Mechanics*, 122 (1982) 467-486.
[25]R. B. Green, and J. H. Gerrard, Vorticity measurements in the near wake of a circular cylinder at low Reynolds numbers, *Journal of Fluid Mechanics*, 246 (1993) 675-691.

Author information

Erika Sandoval Hernandez is a post-doctor of the Exact Sciences Department, CUC, Universidad de Guadalajara, Mexico. She received his Ph.D in Physical-Mathematical Sciences at CU-Valles, Universidad de Guadalajara. Her research interests are ocean and laboratory vortices, fluid-structure interaction, mesoscale eddies and their interaction with the topography.

Stefan G. Llewellyn Smith is a professor in the Department of Mechanical and Aerospace Engineering at UCSD and at Scripps Institution of Oceanography. He received his undergraduate and graduate degrees in mathematics and applied mathematics from the University of Cambridge. His research interests include fluid dynamics, physical oceanography and asymptotic and complex variable methods.

Anne Cros is a titular professor of the Physics Department of Guadalajara University, Mexico. She received her Ph.D in Université Aix-Marseille, France. Her research interests include fluid-structure interaction, transition to chaos and rotating flows.